

Polyaniline/ZnO composites prepared via a green route for sunlight-driven photocatalytic efficient decolorization of methyl orange dye

Yasmine Kadri^{a,b,*}, Ezzeddine Srasra^a, Imen Bekri-Abess^a

^aLaboratory of Composite Materials and Clay Minerals, National Center of Materials Research, Borj Cedria Technopole, Tunis, Tunisia, emails: yasmine.kadri@fst.utm.tn (Y. Kadri), srasra.ezzeddine@gamil.com (E. Srasra), bekrimene@gmail.com (I. Bekri-Abess)

^bFaculty of Sciences of Tunis, University of Tunis El Manar, Tunis, Tunisia

Received 29 November 2021; Accepted 29 July 2022

ABSTRACT

Hybrid composites formed by semi-conductor metal oxide (ZnO) and conducting polymer (PANI) were prepared by simple, efficient, low-cost and environmentally-friendly methods, namely mechano-chemical reaction and a solution combustion synthesis. X-ray diffraction, scanning electron microscopy, Fourier-transform infrared spectroscopy, UV-Visible, laser granulometry, Raman and photoluminescence (PL) spectroscopies were carried out to study the effect of both the grinding time and weight percent ratio of ZnO:PANI on the structure and morphology of ZnO/PANI composites. The X-ray diffraction results show that solution combustion synthesis gave a wurtzite hexagonal structure of pure ZnO and ZnO/x wt.% PANI composites contained zinc oxide with a semi-crystalline phase of polyaniline. Experimental findings demonstrate that the decrease of the grain size particles from 42.15 to 24.49 μm , for ZnO/60 wt.% PANI and the grinding time increase were accompanied by the reduction of PL intensity and electron-hole recombination. The effect of the percentage of polyaniline in the composites on the photodegradation reaction of methyl orange (MO) was also investigated. UV-Vis spectrophotometer findings reveal the adsorption of UV irradiation by all composites and, hence, the decomposition of MO. ZnO/60 wt.% PANI showed good photocatalytic behaviour towards MO dye with a decoloration percentage of 90% after being exposed to sunlight irradiation during 1 h. This rate is six times higher than ZnO in the same conditions. It was obvious that the prolongation of the charge-carrier recombination time, resulting from sensitizing by polymer and activation by grinding, improved the efficiency of the studied composites towards the photocatalytic degradation of MO.

Keywords: Polyaniline; ZnO; Mechano-synthesis; Solution combustion synthesis; Photocatalysis; Decolorization

1. Introduction

In recent years, the quality of water has become more polluted due to the industrial development, agricultural activities and the use of pesticides, herbicides, nitrates, organic dyes, heavy metals, acids and hydrocarbons. As a solution, the concentration of these damaging substances should be minimized physically, by membrane filtration [1], chemically, by ozonation [2], or physico-chemically by coagulation-flocculation [3]. However, the limitation

of membranes activity and the expensive cleaning make this solution less useful. Moreover, the expensive coagulation operation and non-reusability of coagulants, on the one hand, and the high investments and operating costs together with the unknown oxidation products, on the other hand, reduce the efficiency of the coagulation-flocculation technique and that of ozonation method, respectively. To overcome the above-mentioned weaknesses, photocatalysis is as a more useful approach. Beside, metal oxides, used as photocatalysts, are good candidates

* Corresponding author.

due to their important optical and electronic properties [4]. For instance, TiO_2 has shown high efficiency in removing pollutants [5]. Nickel oxide [6], silver tungstate [7], cerium oxide [8], and spinel ferrite [9] have also given good results in dyes degradation. Added to that, zinc oxide (ZnO), a wide band gap n-type semi-conductor, is a potential material for photocatalysis thanks to its high binding energy of excitation of ~ 60 meV, excellent piezo/pyro-electricity properties, low toxicity, chemical/physical stability and bio-compatibility [10]. However, its photocatalytic activity is very limited under natural sunlight irradiation [11], which requires the use of harmful UV lamps. Therefore, for environmental and health reasons, it is necessary to move the photo-activation region of the ZnO nanoparticles to the visible wavelengths. Another solution consists in using photocatalysts under solar radiation, which can be achieved by surface modification of ZnO nanoparticles with the addition of various materials. In this context, different methods, such as doping with noble metals, rare earth elements, nitrogen and sulfur elements [12,13], have been applied. Combining ZnO with another semi-conductor is also another promoting solution. Ghaderi et al. [10] studied the photo-decomposition of methylene blue (MB) and methyl orange (MO) by hybridizing zinc oxide with another semi-conductor (SnO_2) [10]. In another research work, Sharma and Basu [14] successfully synthesized $\text{MoO}_3/\text{SiO}_2$ monoliths by wet impregnation route. The photo-activity of the catalyst was tested through the photodegradation of Rhodamine B dye (RhB). Moreover, the obtained efficiency ratio was equal to 88.6%.

In addition, loading semi-conductors with carbon-based materials showed high efficiency in minimizing the amount of pollutants. In their study, Dashairya et al. [15] anchored antimony sulfide (Sb_2S_3) onto reduced graphene oxide in order to degrade Rhodamine B dye. They eliminated 89% of the pollutant after 150 min of exposure to sunlight irradiance. In another work, Kundu et al. [16] conglomerated $\text{g-C}_3\text{N}_4$ nanosheets with BiOCl nanoplates to degrade MB under sunlight irradiation. The photocatalyst gave a degradation rate equal to 94.8%. However, this value declined to 75% after re-using the catalyst 5 times in a row. In another report Monga et al. [17], a degradation rate equal to 98.7% was obtained when $\text{MoS}_2/\text{g-C}_3\text{N}_4$ (MSC) was utilized as a photocatalyst to eliminate methylene blue dye.

In particular, the hybridization of zinc oxide with conjugated conductive polymers allows increasing considerably the photocatalytic performance since the combination of a p-type conducting polymer and an n-type semi-conductor metal oxide is an efficient method to prevent the recombination of the photo-generated electron-hole pairs due to the absorption in the visible range [18]. Among these polymers, polyaniline is the most widely studied thanks to its reversible redox doping/de-doping chemistry, stability, ease of synthesis, low cost, electrical conductivity and high absorption in the visible region [19].

Besides, the photocatalytic activity of ZnO is also affected by purity of the latter, its particle size, its shape and its crystal defects. These elements, are mainly modulated through the used synthesis method [20]. In the literature, ZnO/PANI composites were prepared using various techniques. For example, Zou et al. [21] prepared pompon-like

ZnO/PANI heterostructure by hydrothermal method and hybridization in THF solvent to treat water pollutants under visible light. Saravanan et al. [22] fabricated ZnO/PANI composites by precipitation followed by a sonication process in diethylene glycol. Moreover, Singh and Choudhary [23] prepared Ag/AgCl sensitized PANI/ZnO composites by in-situ polymerization for hybrid solar cell application. These studies showed that the prepared ZnO/PANI composites have different optical and photodegradation activities. However, the majority of the performed synthesis suffer essentially from the use of pollutant organic solvents.

In comparison with the conventional synthesis methods, solution combustion synthesis (SCS), which is easy to prepare, eco-friendly and time/energy-saving [24], allows obtaining materials dotted with various physico-chemical properties. In addition of being a green and easy synthesis method, it was shown that mechano-chemical activation of ZnO by grinding can affect the particle size, the surface area, photoluminescence, the electron-hole recombination and, thus, the photocatalytic activity [25]. Based on these hypotheses, photocatalytic activity can be enhanced by preventing the easy charge transfer across the layer.

The aim of this study is to develop a green and efficient technique easily utilized to prepare ZnO/PANI composites to be used as photocatalysts. In the performed experiments, oxidative polymerization method was employed to elaborate polyaniline. Then, zinc oxide was rapidly synthesized by a solution combustion synthesis. Both materials (polyaniline and zinc oxide) were hybridized by a mechanical grinding process with different percent ratios of ZnO and PANI and various grinding time. Their photocatalytic efficiency was tested by studying the degradation reaction of methyl orange (MO) under solar radiation.

2. Experimental

2.1. Materials

Zinc nitrate hexahydrate ($\text{Zn}(\text{NO}_3)_2 \cdot 6\text{H}_2\text{O}$, 98%), aniline chloride (AnCl, 97%) and hydrochloric acid (HCl, 37%) were purchased from Sigma-Aldrich (Germany). Ammonia (NH_3 , 28w/w) and ethanol ($\text{C}_2\text{H}_6\text{O}$, 99.9%) were provided from Scharlau. Urea ($\text{CO}(\text{NH}_2)_2$, 99.5%) and ammonium peroxidase (APS, 98.1%) were purchased from Novachim and AnalaR NORMAPUR, respectively. All chemicals were used without any further purification and prepared in double-distilled water.

2.2. Synthesis of ZnO powder

In a previous work, the synthesis of ZnO was reported by a combustion solution synthesis [26]. 3.65 g of $\text{Zn}(\text{NO}_3)_2 \cdot 6\text{H}_2\text{O}$ (used as an oxidant) and 1.23 g of urea (utilized as a fuel) were dissolved in 5 mL of distilled water. The fuel-to-oxidizer ratio ϕ was equal to 1. Ammonia was added to the solution in order to adjust the pH to 7. After complete homogenization, the mixture was introduced, for 10 min, into a preheated muffle furnace and maintained at 400°C . After its transformation into a gel, a quick explosion, accompanied by a significant release of gas, was initiated spontaneously. To assure good crystallinity and purity of zinc oxide, the sample were calcined at 700°C for 2 h.

2.3. Synthesis of PANI and ZnO/PANI composites

2.3.1. Synthesis of PANI

Polyaniline was synthesized by an oxidative polymerization solution method. An aqueous solution of aniline hydrochloride was prepared in double distilled water and a precise mass of ammonium peroxidase was dissolved in water. Then, it was added drop by drop to the aniline monomer solution. The molar ratio of An to APS was 1.0:1.25 [27]. The mixture was polymerized at room temperature without stirring. After that, the solution was filtered in Büchner funnel and the dark blue residual of PANI was washed several times with diluted hydrochloric acid solution (0.1 M) (Sigma-Aldrich 37%) and ethanol (Scharlau 99.9%) to obtain the emeraldine salt form of polyaniline. Finally, the filtered polymer was dried in an oven at 45°C for 24 h.

2.3.2. Synthesis of ZnO/PANI nanocomposites

ZnO/polyaniline nanocomposites were prepared by mechanically mixing ground solids. To synthesize zinc oxide/polyaniline composites, ZnO and PANI with different weight percent ratios were grinded in an agate mortar at various time periods ranging from 5 to 15 min. The used samples are denoted ZnO/*x*% PANI, where *x* represents the weight percent ratio of PANI in the composite.

2.4. Characterization techniques

X-ray diffraction was carried out in 2θ range of 10°–70° by an X-ray diffractometer using Cu K_α radiation (λ = 0.15418 nm, ADVANCE Bruker). Fourier-transform infrared spectra of ZnO, PANI and ZnO/PANI nanocomposites were obtained in the frequency range of 400–4,000 cm⁻¹ employing BX PerkinElmer Spectrometer and KBr pellets. The granulometric distributions of samples were measured using a Laser Granulometer Microtrac S3500. Photoluminescence measurements were performed on a PerkinElmer LS-55 Fluorescence Spectrometer excited at 325 nm at room temperature. The Raman spectra of the examined samples were recorded by a Raman LabRAM HR Spectrometer from HORIBA Jobin Yvon with a laser HeNe of 633 nm. Then, the UV-Visible spectra of the samples were conducted utilizing a PerkinElmer UV-Vis Spectrometer (Lambda 950). Morphological studies were investigated by a scanning electron microscopy (SEM) apparatus FEI Quanta 650 coupled with energy-dispersive X-ray spectroscopy (EDX) and a transmission electron microscopy (TEM) in a JEOL-1010 Microscope (JEOL USA, Inc., Peabody, MA, USA). In order to identify the photodegradation products a GC/MS QP-5000 Shimadzu Mass Spectrometer was used.

2.5. Photodegradation experiments

2.5.1. Preparation of methyl orange solutions

Methyl orange, C₁₄H₁₄N₃NaO₃S (MO), with molecular weight of 327.33 g/mol, is a water soluble dye. MO dye solution was prepared by dissolving a precise amount of MO in bi-distilled water to obtain a solution with a concentration of 25 mg/L.

2.5.2. Determination of photocatalytic activities

MO solutions, with concentration of 25 mg/L and 100 mL of volume, were mixed with 0.075 g of different photocatalysts at a pH = 4. Subsequently, they were kept in dark for 2 h at room temperature to ensure an adsorption-desorption equilibrium between the photocatalyst surface and MO dye. After that, they were exposed to solar radiation at National Center of Materials Research where temperature $T = 35^{\circ}\text{C} \pm 2^{\circ}\text{C}$. As the reaction proceeded and at 30 min of regular intervals, 1 mL of photocatalyst and dye solution was extracted and separated by a centrifuge at a speed of 3,000 rpm. The dye concentration was determined using UV-Visible spectrophotometer at λ_{max} of 464 nm while the decolorization efficiency was specified applying the following equation:

$$\begin{aligned} \text{Decolorization efficiency (\%)} &= \left(\frac{C_0 - C}{C_0} \right) \times 100 \\ &= \left(\frac{A_0 - A}{A_0} \right) \times 100 \end{aligned} \quad (1)$$

where C_0 denotes the initial concentration of the dye solution, C represents the variable concentrations of MO solutions at time t , A_0 corresponds to the initial absorbance, and A is the variable absorbance at time t .

3. Results and discussion

3.1. Structural studies

3.1.1. Fourier-transform infrared spectroscopy

ZnO synthesized by combustion synthesis was characterized using a Fourier-transform infrared spectroscopy (FTIR) technique. Fig. 1a shows the FTIR spectrum of the prepared ZnO. The main peak, corresponding to the $\nu_{(\text{Zn-O})}$ modes and showing the formation of ZnO oxide, is observed at 500 cm⁻¹. The peak of weak intensity, reported at 1,042 cm⁻¹, shows the presence of carbonate ions (CO₃²⁻) [28]. The band at 1,386 cm⁻¹ is assigned to the C–O stretching mode. The bands observed at 3,432 and 2,926 cm⁻¹ reveal the O–H and C=O stretching vibration adsorptions, respectively [29]. These residues may be attributed to the moisture and the fuel carboxyl groups (urea) [30]. The band indexed at 1,644 cm⁻¹ characterizes H–O–H bending assigned to water adsorbed on the surface of ZnO [31].

As demonstrated by Fig. 1a, PANI exhibits characteristic peaks at 3,458; 2,932; 1,586; 1,491; 1,310 and 1,129 cm⁻¹. The intense band situated at 3,458 cm⁻¹ results from the N–H stretching mode [32]. The peak observed at 2,932 cm⁻¹ corresponds to the C–H bonding ring [33]. In addition, the bands indexed at 1,586 and 1,491 cm⁻¹ are related to the stretching vibration modes of the C=N and C=C bonds of the quinoid and benzenoid units, respectively [34]. Moreover, the adsorptions reported at 1,310 and 1,129 cm⁻¹ show the C–N bonding of the benzenoid and quinoid units of PANI. The presence of these units confirms the formation of PANI in its emeraldine salt form. Those results are consistent with those obtained in literature [32,35].

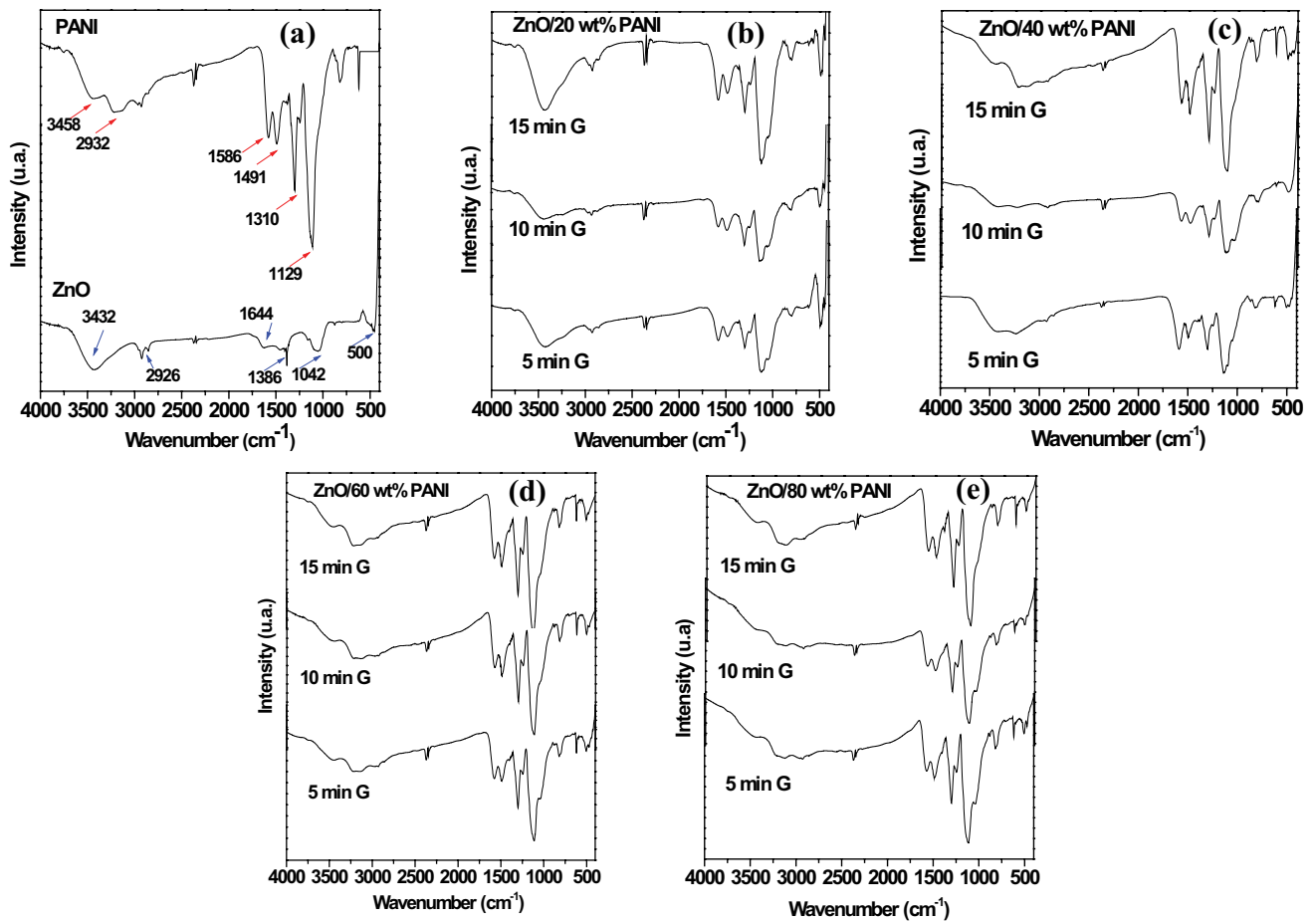


Fig. 1. FTIR spectra of (a) ZnO, PANI, (b) ZnO/20 wt.% PANI, (c) ZnO/40 wt.% PANI, (d) ZnO/60 wt.% PANI and (e) ZnO/80 wt.% PANI nanocomposites.

FTIR analyses were also carried to examine the interaction between ZnO and PANI compounds. It is obvious that ZnO/PANI nanocomposites (Fig. 1b–e) exhibit almost similar IR bands of pristine PANI with a small shift to lower wave numbers. The peaks of pure PANI localized at 1,586; 1,491; 1,310 and 1,129 cm^{-1} shift to 1,580; 1,487; 1,305 and 1,126 cm^{-1} in ZnO 20, 40, 60 and 80 wt.% PANI spectra, respectively. This shift may be attributed to the interactions between the PANI chains and ZnO nanoparticles, resulting from the formation of hydrogen bonding between the O–H group of ZnO and the N–H group of PANI [35].

3.1.2. Powder X-ray diffraction

Fig. 2 shows the X-ray diffraction (XRD) pattern of pure PANI, ZnO and ZnO/PANI nanocomposites. Patterns presented in Fig. 2a demonstrate two characteristic peaks of the emeraldine salt form of PANI at $2\theta = 21.7^\circ$ and 27.3° . These peaks correspond to the parallel and perpendicular periodicity to the polymer chains, respectively [32,34]. The XRD patterns of ZnO sample calcined at 700°C are exposed in Fig. 2b. Well-defined diffraction peaks are noticed in the pattern at 31.8° , 34.5° , 36.3° , 47.5° , 56.6° , 62.8° , 66.4° , 67.9° and 69.1° . These positions are ascribed to the lattice planes

of (100), (002), (101), (102), (110), (103), (200), (112) and (201), respectively [36]. The observed diffraction reflections correspond to the wurtzite hexagonal phase of ZnO. No characteristic diffraction peak of secondary phases is noted, which confirms the purity of the synthesized products.

The average crystallite size was estimated using the following Scherrer formula:

$$D = \frac{k\lambda}{\beta \cos\theta} \quad (2)$$

where k is the Scherrer constant (0.9), λ denotes the wavelength (nm), β corresponds to the peak width at half maximum (FWHM) and θ designates the Bragg diffraction angle ($^\circ$).

The average crystallite size of ZnO was equal to 9 nm. From XRD patterns of ZnO/PANI nanocomposite (Fig. 2c–f), characteristic peaks of PANI and ZnO, confirming the formation of nanocomposites with high crystallinity, are clearly seen. A significant increase in the intensity of PANI peaks and a rising weight percentage of PANI in the nanocomposites are also observed. It is worth noting that the characteristic peaks of ZnO nanoparticles shift negligibly to lower angles after being combined with PANI phase, which

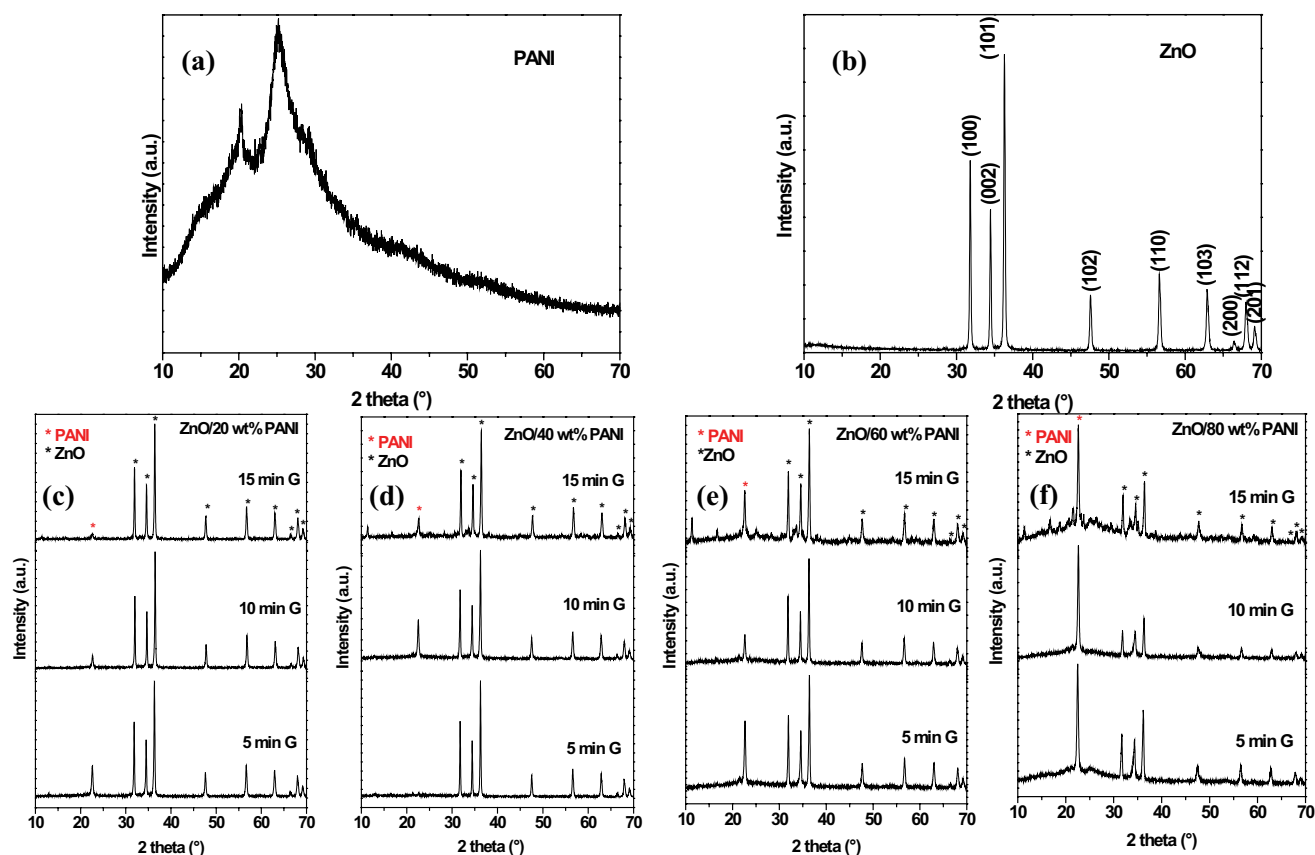


Fig. 2. XRD patterns of (a) PANI, (b) ZnO, (c) ZnO/20 wt.% PANI, (d) ZnO/40 wt.% PANI, (e) ZnO/60 wt.% PANI and (f) ZnO/80 wt.% PANI nanocomposites.

indicates the incorporation of PANI chains between the spaces of crystalline planes in ZnO structure [37].

3.1.3. Raman spectroscopy

Raman spectra of ZnO, PANI and ZnO/PANI samples were recorded to provide information about the interaction between PANI and ZnO nanomaterials. Raman spectrum of pure ZnO is illustrated in Fig. 3a. The intensive band observed at 439 cm^{-1} is attributed to the high nonpolar vibration mode of the optical photons, typical for a wurtzite phase, resulting from the presence of oxygen atoms in ZnO [38]. In addition, the weak peak appearing at 580 cm^{-1} can be assigned to E1 (LO) mode and is related to oxygen deficiency in ZnO samples [39]. In Fig. 3b, five peaks indexed at $1,160$; $1,236$; $1,384$ and $1,514$ – $1,590\text{ cm}^{-1}$, corresponding respectively to C–H stretching vibrations of benzenoid and quinoid rings, C–N benzenoid stretching, CN quinoid stretching and C=C quinoid stretching [40], are observed for pristine PANI. Moreover, it is important to note that the noise in most of Raman peaks increases with the rise of wt.% of PANI (Fig. 3c). A shift of the bands of PANI indexed at $1,514$ and $1,236\text{ cm}^{-1}$ toward lower wavenumbers of about 44 and 16 cm^{-1} , respectively, is also observed due to the strong interaction between PANI and ZnO caused by hydrogen bonding between imine groups of PANI and hydroxyl groups of ZnO [39].

3.1.4. Grain size analysis

The effects of wt.% of PANI and grinding time on the particle-size distribution, the evolution of the percentage of fine particles and the peak of the different samples distribution are presented in Fig. 4. The particle-size distribution of ZnO shows a bimodal distribution with two maxima at 0.5 and $3.6\text{ }\mu\text{m}$. However, the particle-size distribution of PANI has only one maximum at $23\text{ }\mu\text{m}$. The particle-size distribution could be grouped into two categories: sizes inferior to $1\text{ }\mu\text{m}$ (ultrafine and fine particle) and sizes above $1\text{ }\mu\text{m}$ (coarse particle). In the case of ZnO/40 wt.% PANI, and after 5 min of grinding, all particles are classified into coarse range. However, after 15 min of grinding, 10% of the particles are in the fine range and 90% of the particles are in the coarse range. Particle size reduction can be explained by the breaking up and fracture of coarse particles into finer ones under grinding strain. Table 1 regroups the size distribution of all the composites at different grinding times.

3.2. Morphological study

In order to investigate the morphology of our samples, SEM and TEM images of ZnO nanoparticles, synthesized by combustion synthesis at $\text{pH} = 7$ and calcined at 700°C for 2 h, the pristine PANI, elaborated through an in-situ polymerization, and the ZnO/PANI composites,

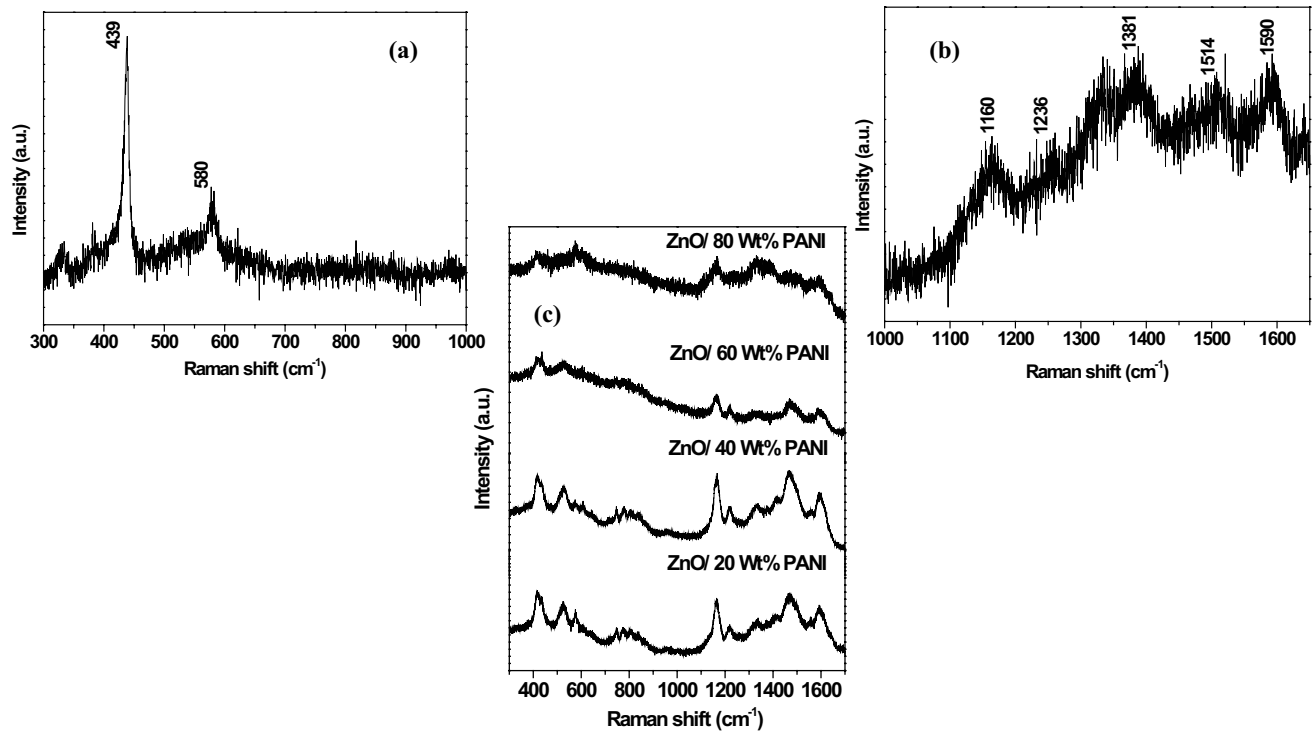


Fig. 3. Raman spectra of (a) ZnO, (b) PANI and (c) ZnO/PANI nanocomposites.

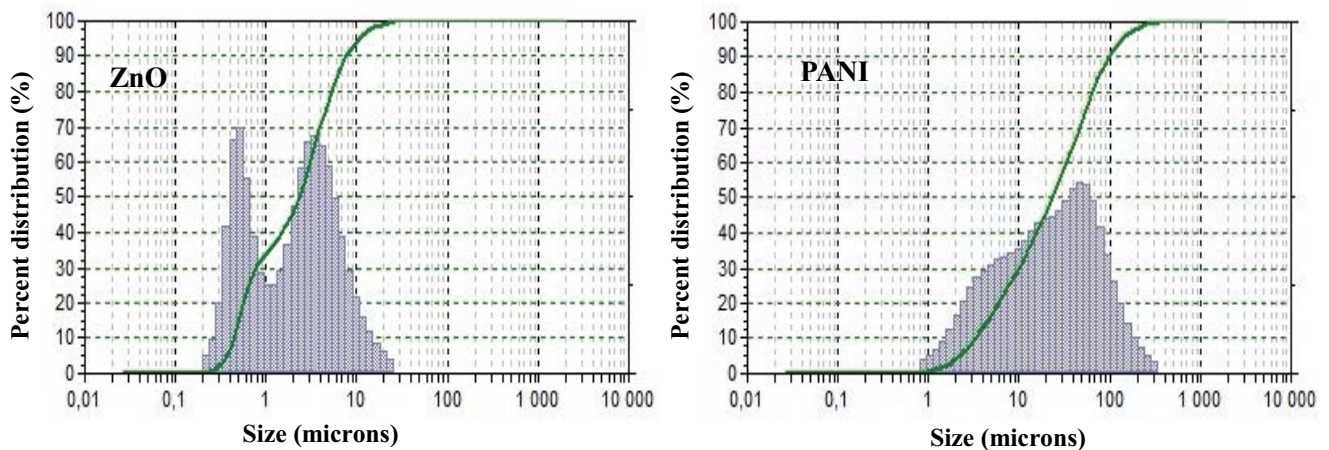


Fig. 4. Particle-size distribution of ZnO and PANI.

grinded for 15 min, were examined. ZnO nanoparticles with diameters ranging between 300 and 450 nm are exposed in Fig. 5a and g. The performed analysis reveals the agglomeration of those nanoparticles. A sheet-like morphology of PANI is also presented in Fig. 5b. Comparison between ZnO and ZnO/PANI composite demonstrates more accumulation in the morphology of the studied composites, which is attributed to the interaction between ZnO and PANI (Fig. 5c–f). An EDX analysis of different samples is revealed in Fig. 6. The weak sulfur and nitrogen peaks indexed in EDX spectra of PANI and ZnO/PANI composites (Fig. 6b–f) can be explained by the use of the

oxidant agent (APS) in the synthesis of PANI. The high intensities of Zn, O and C peaks confirm the existence of ZnO nanoparticles in the hybrid structure (Fig. 6c–f).

3.3. Optical studies

3.3.1. Photoluminescence studies

The effect of incorporating PANI and grinding on the separation and time of recombination of the electron–hole pairs of different photocatalysts was studied using room temperature photoluminescence (PL) at an excitation

Table 1
Particle-size distribution of ZnO/x wt.% PANI nanocomposites at different grinding time

Sample	Particle size (μm)
ZnO/20 wt.% PANI 5 min G*	15.11
ZnO/20 wt.% PANI 10 min G	14
ZnO/20 wt.% PANI 15 min G	13.59
ZnO/40 wt.% PANI 5 min G	12.89
ZnO/40 wt.% PANI 10 min G	9.44
ZnO/40 wt.% PANI 15 min G	4.98 (90%) + 0.53 (10%)
ZnO/60 wt.% PANI 5 min G	42.15
ZnO/60 wt.% PANI 10 min G	28.73
ZnO/60 wt.% PANI 15 min G	24.49
ZnO/80 wt.% PANI 5 min G	38.30
ZnO/80 wt.% PANI 10 min G	31.27
ZnO/80 wt.% PANI 15 min G	25.34

B: Grinding

wavelength of 325 nm. Fig. 7a presents the various photoluminescence spectra of ZnO and ZnO/PANI nanocomposites. The PL emission spectra of the several examined samples reveal five emission bands at 400, 458, 482, 524 and 532 nm, respectively. The increase of wt.% of PANI in ZnO/PANI nanocomposites leads to the rise of PL peak intensity and reflects the decrease of electron-hole recombination of different nanocomposites. The same observation was noted in the literature by Salah et al. [41]. This phenomenon can result from the absorption of the light emitted by PANI, attributed to the transfer of electrons from the ZnO nanocrystals to the conducting-holes of PANI, which reduces their luminescence [41]. Furthermore, it is important to note that, for the same weight percent ratio of PANI, the increase of grinding time treatment leads to the decrease of luminescence intensity. A previous study attributed this phenomenon to the rearrangement of ZnO surface particles under grinding strain and to the decrease of the surface defects considered as active sites in the photocatalytic process [42].

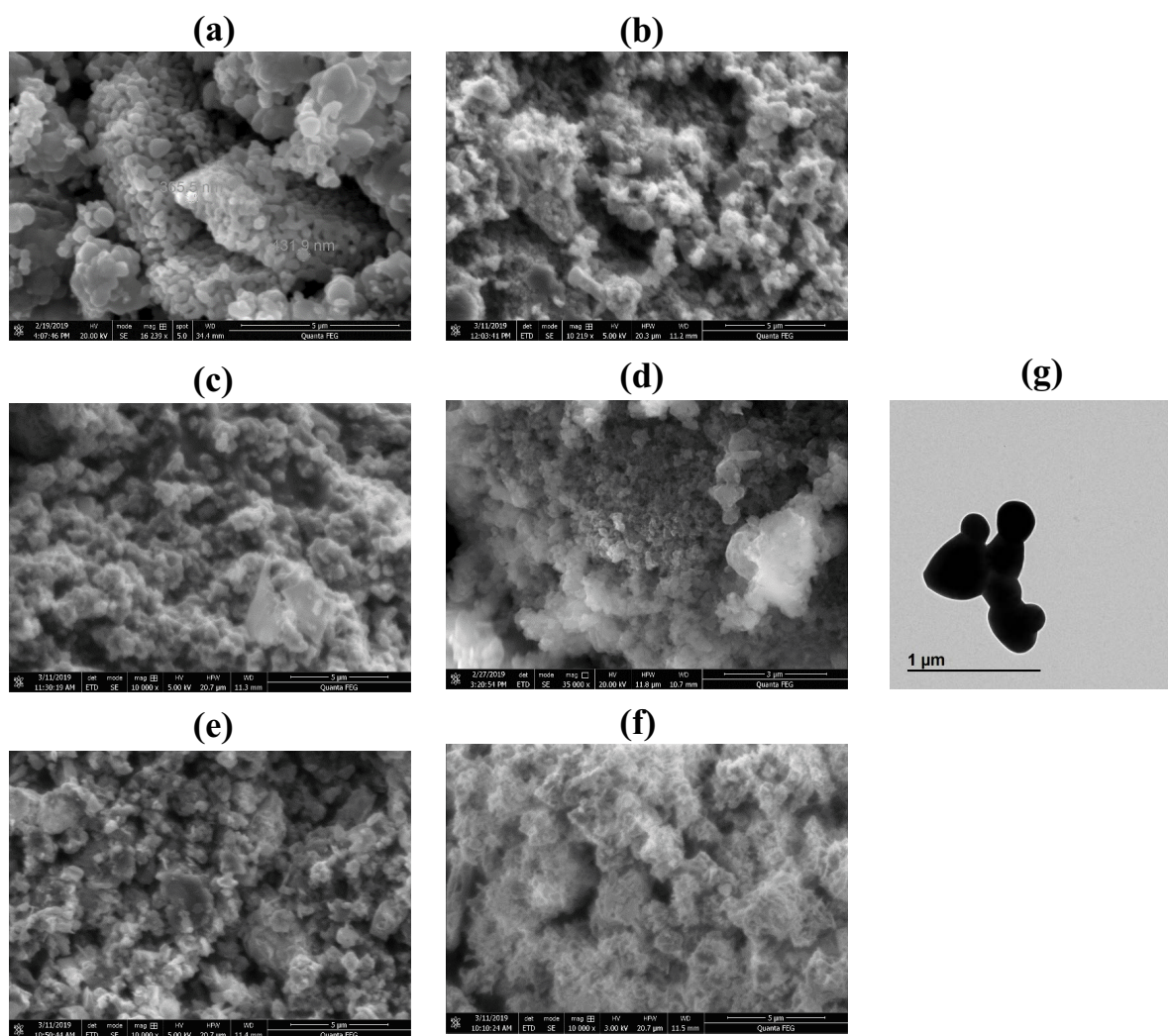


Fig. 5. SEM images of (a) ZnO, (b) PANI, (c) ZnO/20 wt.% PANI, (d) ZnO/40 wt.% PANI, (e) ZnO/60 wt.% PANI and (f) ZnO/80 wt.% PANI nanocomposites and TEM photo of (g) ZnO

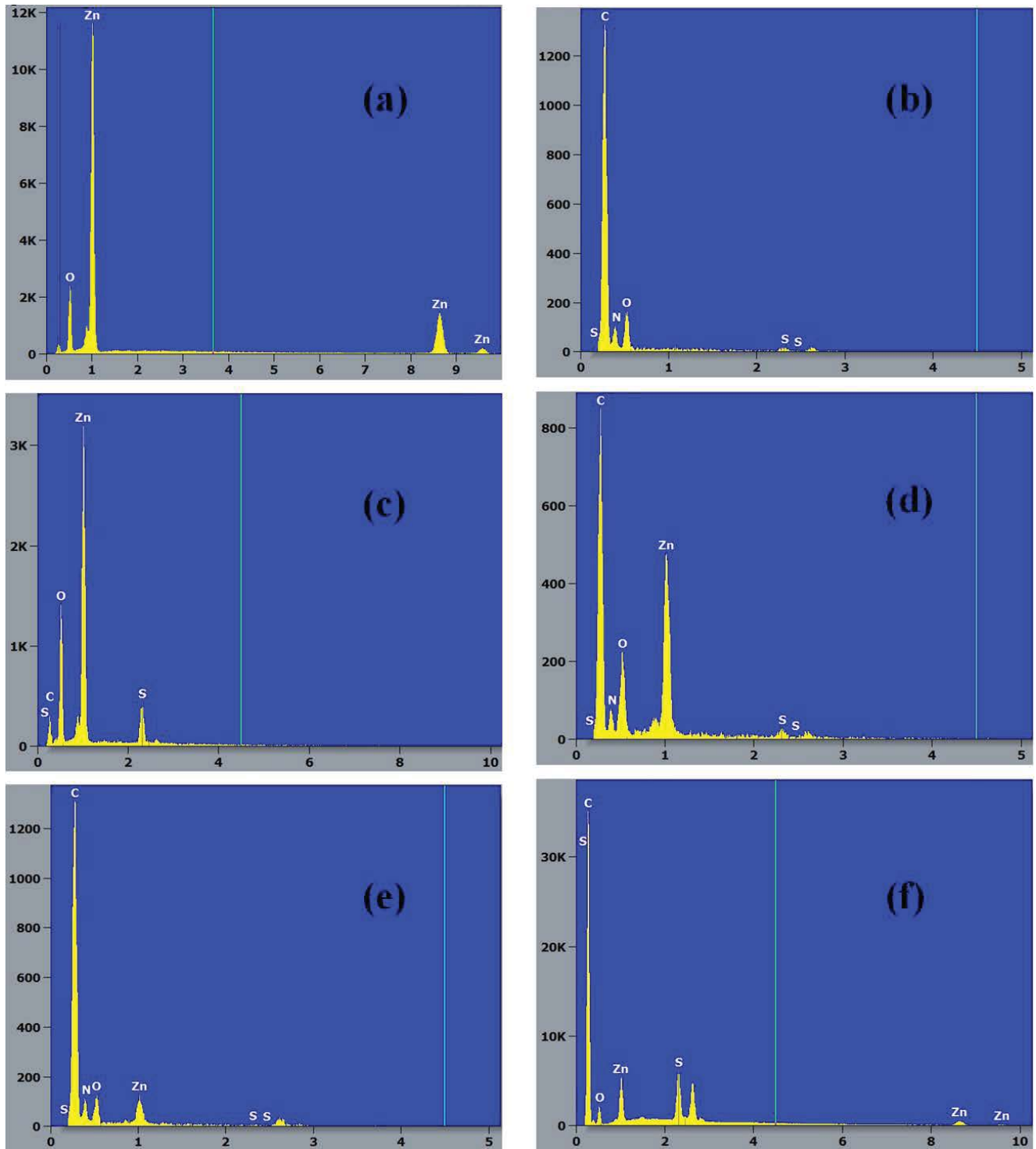


Fig. 6. EDX spectra of (a) ZnO, (b) PANI, (c) ZnO/20 wt.% PANI, (d) ZnO/40 wt.% PANI, (e) ZnO/60 wt.% PANI and (f) ZnO/80 wt.% PANI nanocomposites.

3.3.2. UV-Visible spectroscopy

The recorded UV-Visible spectra of ZnO nanoparticles, pristine PANI and ZnO/PANI nanocomposites are presented in Fig. 8. ZnO nanoparticles show, in Fig. 8a, a strong broad

peak in UV region between 300–381 nm, which confirms the wurtzite hexagonal structure reported previously by X-ray diffraction [32]. In Fig. 8b, pristine PANI spectrum demonstrates three large bands located at 313, 356 and 620 nm attributed respectively to $\pi \rightarrow \pi^*$ transitions of benzenoid

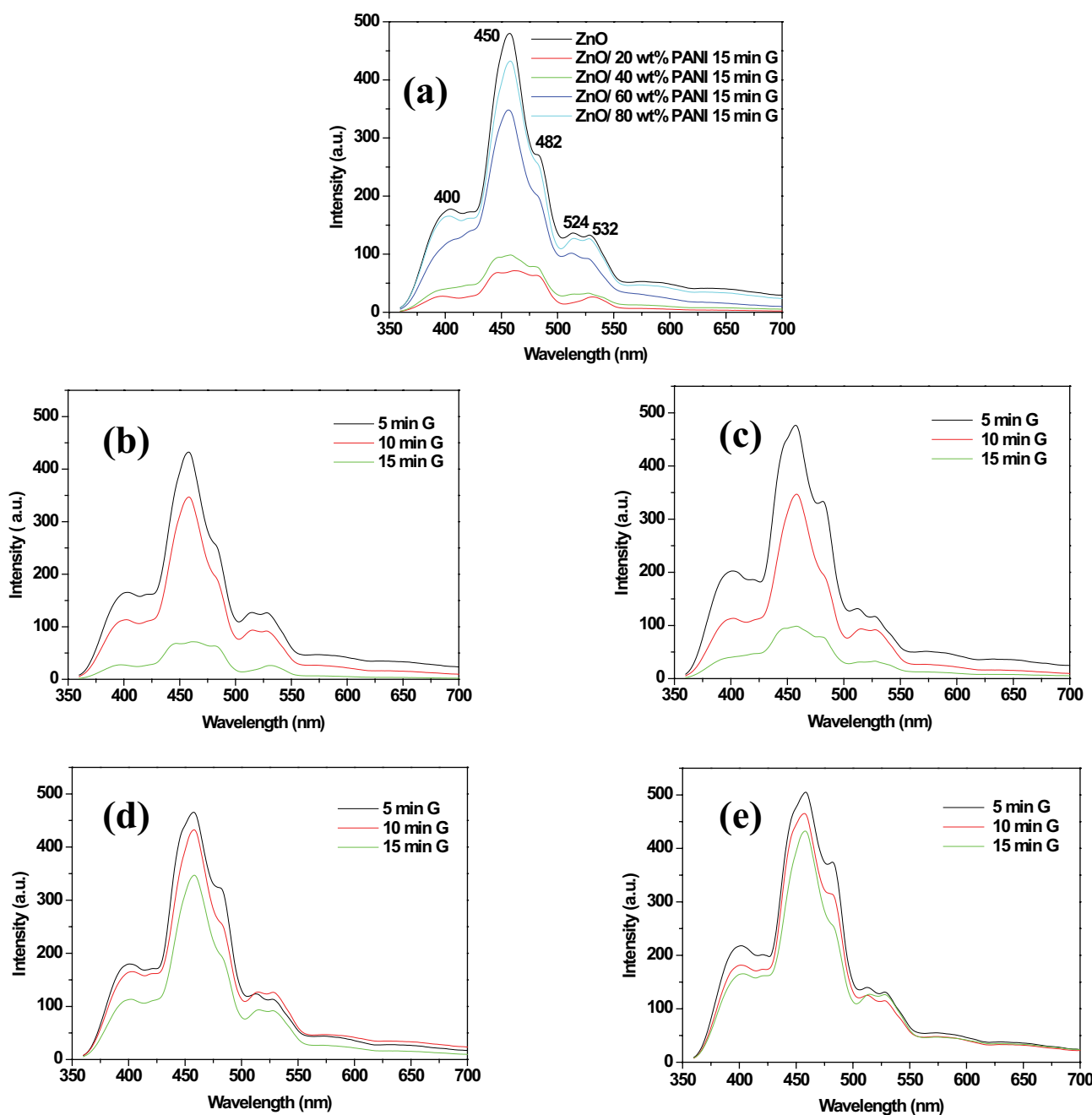


Fig. 7. Photoluminescence spectra of (a) ZnO/wt.% PANI, (b) ZnO/20 wt.% PANI, (c) ZnO/40 wt.% PANI, (d) ZnO/60 wt.% PANI and (e) ZnO/80 wt.% PANI nanocomposites.

segments and $n \rightarrow \pi^*$ transitions due to the doping level and polaron formation into emeraldine form of polyaniline [43]. These three peaks indicate that PANI can absorb light in both UV and visible light regions of the spectrum. The increase of the weight percent ratio of PANI in ZnO/PANI nanocomposites lead to the rise in the peaks intensities (Fig. 8c). A considerable red shift from 620 to 526 nm, explained by the interaction between ZnO nanoparticles and PANI chains via hydrogen bonding, is also observed.

The electronic band gap of pure ZnO nanoparticles and ZnO/PANI composites was calculated because of their

important role in improving the photocatalytic properties of the studied samples. The band gap energy (E_g) was estimated by Kubelka–Munk theory using the following equation:

$$F(R) = \frac{(1-R)^2}{2R} \quad (3)$$

with $[F(R) h\nu] = A(h\nu - E_g)$ where $F(R)$ is the Kubelka–Munk function, R represents the reflectance diffuse. The gap energy (E_g) was estimated by

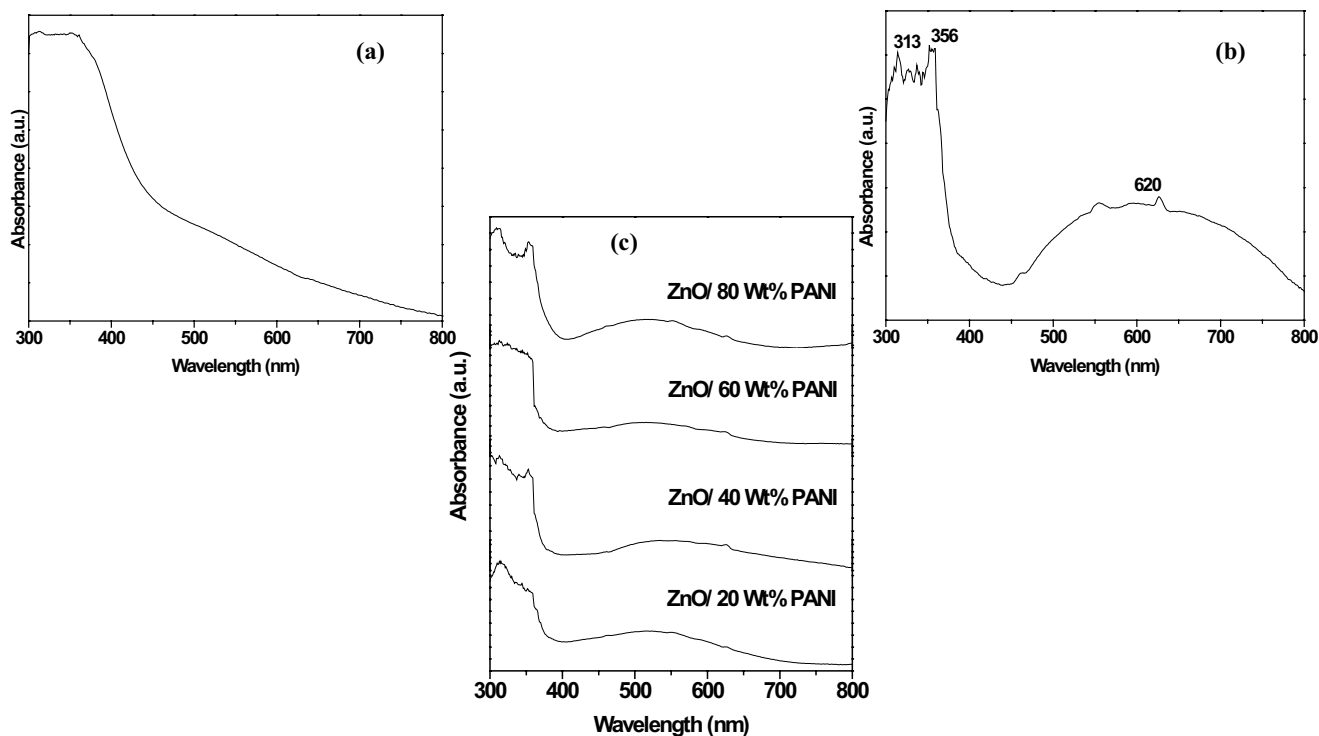


Fig. 8. UV-Vis spectra of (a) ZnO, (b) PANI and (c) ZnO/PANI nanocomposites grinded for 15 min.

extrapolating the linear part of the curve representing $F(R)$ $h\nu = f(h\nu)$ on the axis $h\nu$ (eV).

The band gap of the pure ZnO nanoparticles and pure PANI are 3.12 and 2.75 eV, respectively. The band gap of ZnO/PANI composites decreases with the increase in the percentage of PANI in the composite. The band gaps were estimated to be 2.9, 2.85, 2.65 and 2.6 eV for ZnO/20 wt.% PANI, ZnO/40 wt.% PANI, ZnO/60 wt.% PANI and ZnO/80 wt.% PANI nanocomposites, respectively.

This decrease may facilitate the transfer of electrons from the LUMO band of PANI molecules to the conduction band of ZnO nanoparticles when these composites are used as photocatalysts. Therefore, ZnO/PANI composites can be photoactivated under natural sunlight irradiation.

3.4. Photocatalytic activity

In photocatalytic activity, only ZnO and ZnO/PANI composites prepared by grinding for 15 min were studied. The change in colors and the optical absorption spectra of MO dye solutions in the dark and under sunlight irradiation with different photocatalysts are depicted in Fig. 9. The latter shows that the maximum absorption at $\lambda_{\max} = 464$ nm decreases continuously with the increase of exposure time from 0 to 3 h.

Fig. 10 illustrates the evolution of the decolorization efficiency of MO dye solution for different photocatalysts. In case of PANI, the adsorption of MO in obscurity provided better results and the good adsorption of MO may be due to the high concentration of H^+ on the surface of PANI (sel form), which facilitated the fixation and adsorption of MO dye. The important electrostatic attraction

between the anionic charged MO and the adsorbent positive charged surface is the main reason of this behavior. However, when exposed to solar radiation, the degradation rate is not very important. For this reason, only the photocatalytic properties of ZnO and ZnO/PANI composites are examined in the present research work. Obviously, ZnO nanoparticles show the lowest photocatalytic activity with decolorization efficiency of 15% and 41.5% after 60 and 180 min of exposure to sunlight. This can be attributed to the large band gap of ZnO requiring high energy, which cannot be provided by sunlight radiation, in order to excite electrons from the valence band to the conduction band. After incorporating PANI, different photocatalysts reveal better degradation efficiency and decolorization rate increases with the rise of wt.% of PANI. Compared to ZnO nanoparticles photocatalytic efficiency, the obtained decolorization efficiencies after 60 min of sunlight exposure are 24, 64, 90 and 98.5 for ZnO/20 wt.% PANI, ZnO/40 wt.% PANI, ZnO/60 wt.% PANI and ZnO/80 wt.% PANI, respectively. The enhancement of MO degradation rate with the increase in the amount of PANI in ZnO/PANI composites may be explained by the high photo-generated electron-hole pairs charge separation between pristine PANI and ZnO nanoparticles, which prevented the recombination of electron-hole charge pairs thanks to the process of grinding and to sensitizing by PANI. The absorption of visible light of sunlight was ensured by the interconnection of PANI with ZnO nanopowder [39].

It is interesting to note that these decolorization rates values are greater than those cited in the literature. In his work, Abbasi and Ekrami-Kakhki [44] studied the effects of the photocatalytic properties of multi-walled

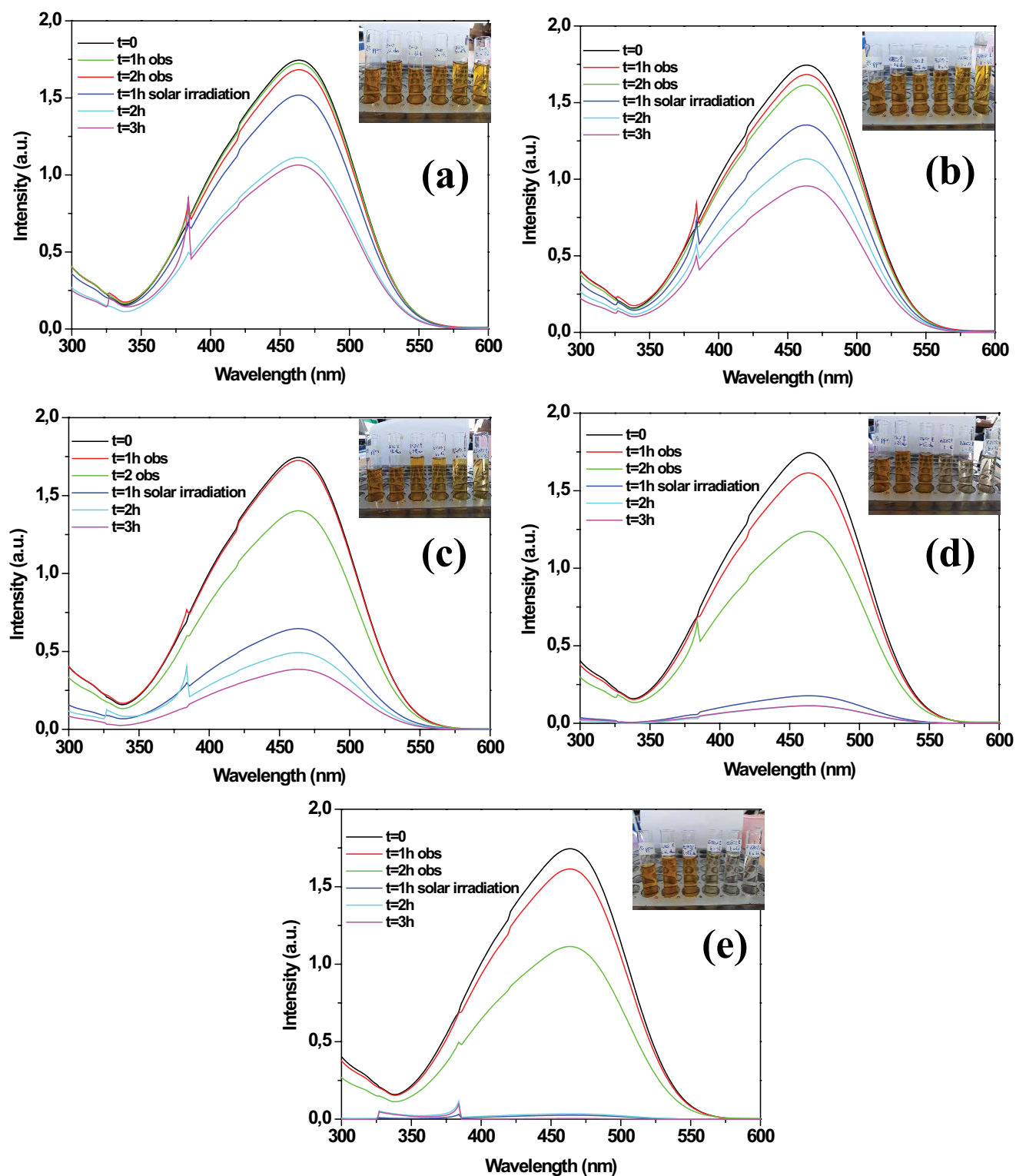


Fig. 9. UV-absorption spectra of MO dye (a) ZnO, (b) ZnO/20 wt.% PANI, (c) ZnO/40 wt.% PANI, (d) ZnO/60 wt.% PANI and (e) ZnO/80 wt.% PANI nanocomposites at obscurity and under sunlight irradiation for different irradiation times.

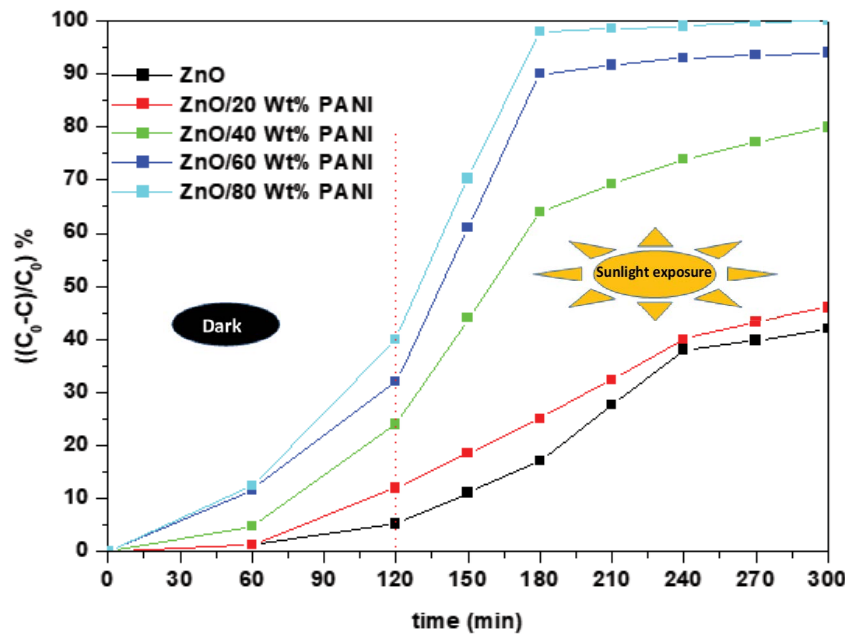


Fig. 10. Extent of decomposition of MO dye with respect to time intervals over ZnO and ZnO/PANI nanocomposites.

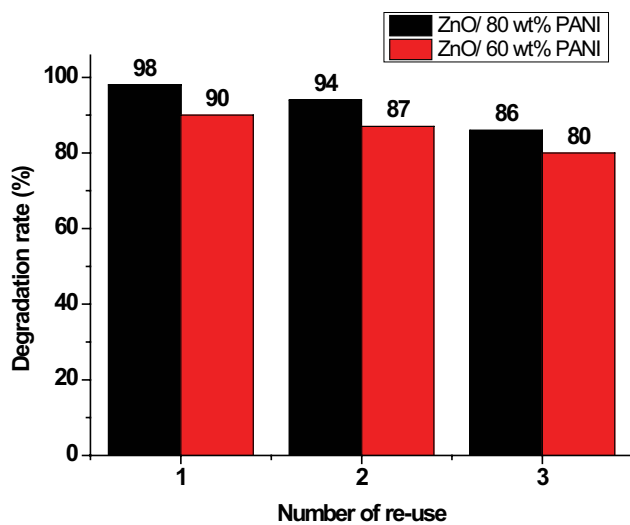


Fig. 11. Three consequent run in photodegradation of MO dye over ZnO/60 wt.% PANI and ZnO/80 wt.% PANI catalysts.

carbon nanotubes (MWCNTs) coupled with zinc oxide nanoparticles on the photodegradation of MO dye. 99.83% of MO dye was removed after 25 min of exposure to a high-pressure mercury vapour lamp (150 W) for an amount of 0.5 g of catalyst and at a pH = 4. It was revealed that the enhancement of the introduced ZnO nanoparticles on the surface of MWCNTs led to the increase of the pollutants removal. In another work, Abbasi [45] successfully synthesized magnetic adsorbents containing ZnO nanoparticles and graphene oxide to be used as photocatalyst in the decomposition of MO. He noticed that MGOZ containing the highest amount of ZnO gave the highest degradation

rate at a pH = 3. Besides, Saravanan et al. [22] studied the degradation of MO dye on 0.1 g of ZnO/PANI nanocomposites prepared by the precipitation of ZnO and sonication with PANI in diethylene glycol solution. The obtained decolorization rate ranged from 15% to 30% after 60 min of exposure to visible light. In the same context, Wondwossen et al. [46] fabricated ZnO/PANI nanocomposites by the precipitation of ZnO and in-situ polymerization with PANI. A decolorization rate for MO of 65% was obtained for an amount of 1.5 g/L of photocatalyst and pH = 6 after 60 min of visible light radiation. El-Khouly et al. [47] showed that ZnO nanoparticles supported on the activated carbon (ZnO-AC) gave high catalytic oxidation of Maxilon red (MR) basic dye at pH = 10 after 150 min of visible light radiation. However, the reusability test demonstrated the decrease of photocatalytic activity from 90% to 72% in the fourth re-use. In their work, Farag et al. [48] used zinc oxide supported on xerogels activated carbon (ZnO-XC-A) as a photocatalyst in the degradation reaction of methyl orange (MO). The degradation rate, that was equal to 98% in the first test after 90 min of exposure to visible light, decreased to 60% in the fifth re-use. In this study, 90% and 98% of a 25 mg/L MO solution degrades by 0.075 g of ZnO/60 wt.% PANI and ZnO/80 wt.% PANI, respectively, at a pH = 4 and after only 60 min under sunlight radiation. The reusability test shows a slight decrease in the degradation rate from 90% to 80% and from 98% to 86% when ZnO/60 wt.% PANI and ZnO/80 wt.% PANI are re-used three times (Fig. 11).

Fig. 12 represents the FTIR spectra of the examined samples after performing photocatalytic tests to evaluate their stability. Similarity between the used composites before and after the photocatalytic decolorization of MO is clearly noted, which indicates their stability during the photocatalytic process.

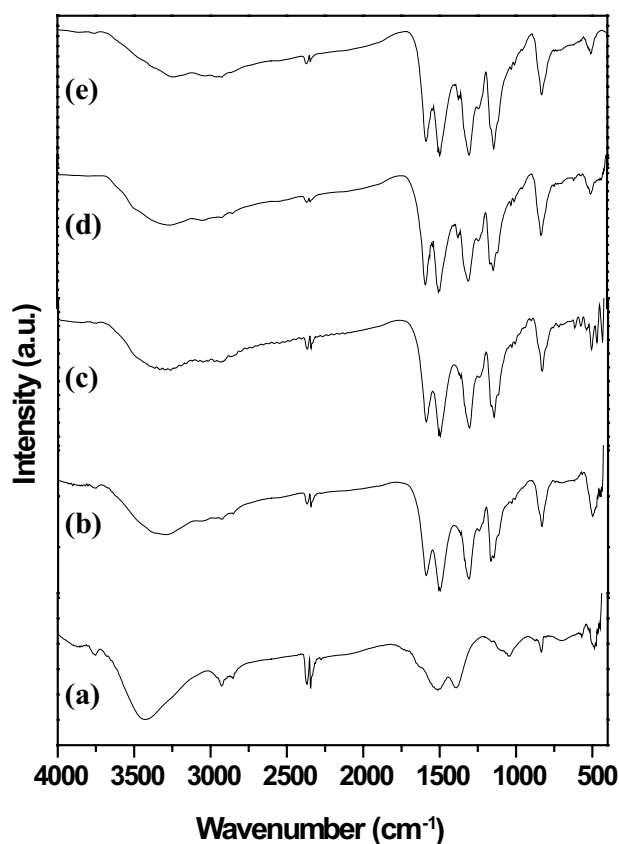


Fig. 12. FTIR spectra of (a) ZnO, (b) ZnO/20 wt.% PANI, (c) ZnO/40 wt.% PANI, (d) ZnO/60 wt.% PANI and (e) ZnO/80 wt.% PANI nanocomposites after photocatalytic degradation of MO dye.

It can be concluded that coating ZnO nanoparticles with PANI chains enhanced its photocatalytic activity under solar radiation. It is also obvious that PANI played the role of a photosensitizer. In accordance with previous reports, Fig. 13 exposes the mechanism of photocatalytic activity of ZnO/PANI nanocomposites under solar radiation [22,39]. When exposed to sunlight irradiance, PANI molecules absorbed photons. Firstly, a photo-excited electron (e^-) was generated from π^* orbital of PANI. Then, it was transferred into ZnO conduction band (CB). This phenomenon was accompanied by the formation of a hole (h^+) in the valence band (VB) of ZnO nanoparticles caused by the transfer of an electron from VB of ZnO to π orbitals of PANI. Subsequently, electrons located in CB of ZnO were transferred to the nanocomposites surface in order to reduce molecular oxygen and produce superoxide radicals $O_2^{\cdot-}$ which reacted with water to form OOH^{\cdot} radical species. At the same time, h^+ holes in VB of ZnO reacted with water to produce OH^{\cdot} radicals. These oxyradicals ($O_2^{\cdot-}$, OH^{\cdot} and OOH^{\cdot}) were capable of reacting with adsorbed MO dye and yielded to MO^+ intermediates that were transformed to the oxidation products.

The degradation products were analyzed by using GC-MS. A probable mechanism is proposed in Fig. 14.

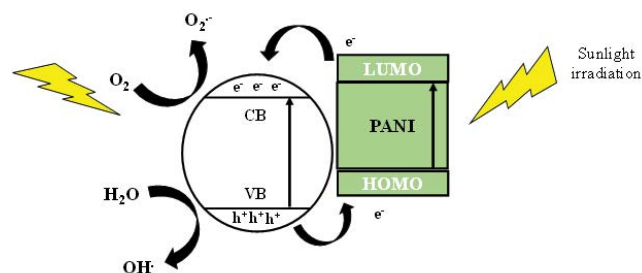


Fig. 13. Mechanism of photocatalytic activity of ZnO/PANI nanocomposites under solar radiation.

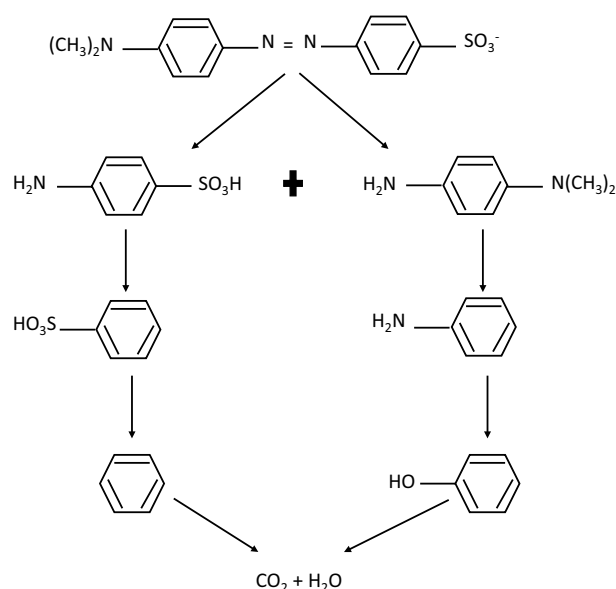


Fig. 14. Degradation mechanism of methyl orange over ZnO/PANI nanocomposites in aqueous solutions.

Before starting the degradation process the sample shows two m/z peaks of high intensity at 304, that correspond to the ionization of MO molecule. After 15 min, two high intensity m/z peaks are observed at 173 and 136. This reduction process is attributed to the symmetric cleavage of azo bond, causing the formation of 4-aminobenzenesulfonic acid and *N,N*-dimethyl-*p*-phenylenediamine [49]. After 30 min, those compounds get converted into aniline (m/z 93) and benzene sulfonic acid (m/z 158). After 45 min, the main fragments are phenol (m/z 94) and benzene (m/z 78). Finally, organic acids are destructed into CO_2 and H_2O after 60 min. This was proven by the indexation of an m/z peak at 44, that corresponds to the CO_2 formation. These results confirmed the total degradation of methyl orange and the formation of intermediates during solar radiation.

The photocatalytic activity of ZnO/PANI nanocomposites was improved by the synergistic effect of PANI and ZnO and the mechano-chemical grinding, which favored the decrease of particles size, the increase of surface area and the introduction of ZnO structural defects influencing positively the photo-generated electron hole recombination

rate. By this way, PANI chains absorbed the light, caused the photo-generation of e^-h^+ pairs charge separation in semi-conductors and increased its lifetime. Thus, the rise in wt.% of PANI in ZnO/PANI nanocomposites generated high number of e^-h^+ pairs and produced a huge amount of oxyradicals (O_2^* , OH^* , OOH^*), which led to a high decolorization rate of MO under sunlight irradiance.

4. Conclusion

In this study, an efficient photocatalyst PANI/ZnO composites was successfully elaborated via a simple and eco-friendly mechanical grinding process. The following conclusions can be drawn from this investigation:

- The structural study of ZnO/PANI nanocomposites showed a significant change when varying the weight percent ratio of pristine PANI and the time of grinding. The good interaction between PANI and ZnO nanoparticles through hydrogen bonding between imine groups of PANI and hydroxyl groups of ZnO was proved by FTIR and Raman spectroscopies.
- The optical investigation revealed a remarkable decrease of electron hole recombination and adsorption of light in a large range of solar spectrum. This reduction was accompanied by the decrease of PL peaks intensity after the rise of the grinding time and the indexation of bands between 300 and 700 nm on UV spectra of the used composites after combining PANI with ZnO.
- For only 60 min of exposure to solar irradiation, 98% and 90% of MO dye solution, with an initial concentration of 25 mg/L, was photo-degraded when 0.075 g of ZnO/80 wt.% PANI and ZnO/60 wt.% PANI were used as photocatalysts. The considerable MO elimination could be caused by the quenching of photo-luminescence, the effective separation of electron/hole and the subsequent reduction in the rate of recombining the charged carriers. It may be attributed to the synergistic effect of PANI and ZnO and to the grinding process.

Acknowledgment

The authors gratefully acknowledge The Tunisian Ministry of Higher Education and Scientific Research for funding this research. A special thank you for Pr. Hanen Walha for the English proofreading.

References

- [1] N. Al-Bastaki, Removal of methyl orange dye and Na_2SO_4 salt from synthetic waste water using reverse osmosis, *Chem. Eng. Process. Process Intensif.*, 43 (2004) 1561–1567.
- [2] F. Zhang, A. Yediler, X. Liang, A. Kettrup, Effects of dye additives on the ozonation process and oxidation by-products: a comparative study using hydrolyzed C.I. Reactive Red 120, *Dyes Pigm.*, 60 (2004) 1–7.
- [3] V. Golob, A. Vinder, M. Simonic, Efficiency of the coagulation/flocculation method for the treatment of dyebath effluents, *Dyes Pigm.*, 67 (2005) 93–97.
- [4] A. Rafiq, M. Ikram, S. Ali, F. Niaz, M. Khan, Q. Khan, M. Maqbool, Photocatalytic degradation of dyes using semiconductor photocatalysts to clean industrial water pollution, *J. Ind. Eng. Chem.*, 97 (2021) 111–128.
- [5] S. Belekbir, M. El Azzouzi, A. El Hamidi, L. Rodríguez-Lorenzo, J.A. Santaballa, M. Canle, Improved photocatalyzed degradation of phenol, as a model pollutant, over metal-impregnated nanosized TiO_2 , *Nanomaterials*, 10 (2020) 996–1022.
- [6] A. Akbari, Z. Sabouri, H.A. Hosseini, A. Hashemzadeh, M. Khatami, M. Darroudi, Effect of nickel oxide nanoparticles as a photocatalyst in dyes degradation and evaluation of effective parameters in their removal from aqueous environments, *Inorg. Chem. Commun.*, 115 (2020) 107867, doi: 10.1016/j.inoche.2020.107867.
- [7] S. Zinatloo-Ajabshir, M. Baladi, O. Amiri, M. Salavati-Niasari, Sonochemical synthesis and characterization of silver tungstate nanostructures as visible-light-driven photocatalyst for wastewater treatment, *Sep. Purif. Technol.*, 248 (2020) 117062, doi: 10.1016/j.seppur.2020.117062.
- [8] Z. Sabouri, M. Sabouri, M.S. Amiri, M. Khatami, M. Darroudi, Plant-based synthesis of cerium oxide nanoparticles using *Rheum turkestanicum* extract and evaluation of their cytotoxicity and photocatalytic properties, *Mater. Technol.*, 37 (2022) 555–568.
- [9] K.K. Kefeni, B.B. Mamba, Photocatalytic application of spinel ferrite nanoparticles and nanocomposites in wastewater treatment: review, *Sustainable Mater. Technol.*, 23 (2020) 140–152.
- [10] A. Ghaderi, S. Abbasi, F. Farahbod, Synthesis, characterization and photocatalytic performance of modified ZnO nanoparticles with SnO_2 nanoparticles, *Mater. Res. Express*, 5 (2018) 1–37.
- [11] Y. Zhang, *ZnO Nanostructures: Fabrication and Applications*, Royal Society of Chemistry, Cambridge, 2017.
- [12] C. Karunakaran, V. Rajeswari, P. Gomathisankar, Optical, electrical, photocatalytic, and bactericidal properties of microwave synthesized nanocrystalline Ag-ZnO and ZnO, *Solid State Sci.*, 13 (2011) 923–928.
- [13] E.U. Umukoro, S.S. Madyibi, M.G. Peleyeju, L. Tshwenya, E.H. Viljoen, J.C. Nagila, O.A. Arotiba, Photocatalytic application of Pd-ZnO-exfoliated graphite nanocomposite for the enhanced removal of acid orange 7 dye in water, *Solid State Sci.*, 74 (2017) 118–124.
- [14] S. Sharma, S. Basu, Visible-light-driven efficient photocatalytic abatement of recalcitrant pollutants by centimeter-length MoO_3/SiO_2 monoliths with long service life, *Appl. Mater. Today*, 23 (2021) 101033, doi: 10.1016/j.apmt.2021.101033.
- [15] L. Dashairya, S. Sharma, A. Rathi, P. Saha, S. Basu, Solar-light-driven photocatalysis by Sb_2S_3 /carbon based composites towards degradation of noxious organic pollutants, *Mater. Chem. Phys.*, 273 (2021) 125120, doi: 10.1016/j.matchemphys.2021.125120.
- [16] A. Kundu, S. Sharma, S. Basu, Modulated BiOCl nanoplates with porous g- C_3N_4 nanosheets for photocatalytic degradation of color/colorless pollutants in natural sunlight, *J. Phys. Chem. Solids*, 154 (2021) 110064, doi: 10.1016/j.jpcs.2021.110064.
- [17] D. Monga, D. Ilager, N.P. Shetti, S. Basu, T.M. Aminabhavi, 2D/2d heterojunction of $MoS_2/g-C_3N_4$ nanoflowers for enhanced visible-light-driven photocatalytic and electrochemical degradation of organic pollutants, *J. Environ. Manage.*, 274 (2020) 111208, doi: 10.1016/j.jenvman.2020.111208.
- [18] A.M. Oves, R. Kumar, M.A. Barak, Fabrication of ZnO-ZnS@polyaniline nanohybrid for enhanced photocatalytic degradation of 2-chlorophenol and microbial contaminants in wastewater, *Int. Biodeterior. Biodegrad.*, 119 (2017) 66–77.
- [19] A. Elschne, S. Kirchmeyer, W. Lövenich, U. Merker, K. Reuter, *Principles and Applications of an Intrinsically Conductive Polymer*, CRC Press: Taylor and Francis Group, Boca Raton FL, 2010.
- [20] L. Zhou, Z. Han, G.D. Li, Z. Zhao, Template-free synthesis and photocatalytic activity of hierarchical hollow ZnO microspheres composed of radially aligned nanorods, *J. Phys. Chem. Solids*, 148 (2021) 109719, doi: 10.1016/j.jpcs.2020.109719.
- [21] T. Zou, C. Wang, R. Tanc, W. Song, Y. Cheng, Preparation of pompon-like ZnO-PANI heterostructure and its applications for the treatment of typical water pollutants under visible light, *J. Hazard. Mater.*, 338 (2017) 276–286.

- [22] R. Saravanan, E. Sacari, F. Gracia, M.M. Khan, E. Mosquera, V.K. Gupta, Conducting PANI stimulated ZnO system for visible light photocatalytic degradation of coloured dyes, *J. Mol. Liq.*, 222 (2016) 1029–1033.
- [23] R. Singh, R.B. Choudhary, Ag/AgCl sensitized n-type ZnO and p-type PANI composite as an active layer for hybrid solar cell application, *Optik*, 225 (2021) 165766, doi: 10.1016/j.ijleo.2020.165766.
- [24] H.V. Vasei, S.M. Masoudpanah, M. Habibollahzadeh, Different morphologies of ZnO via solution combustion synthesis: the role of fuel, *Mater. Res. Bull.*, 125 (2020) 110784, doi: 10.1016/j.materresbull.2020.110784.
- [25] G.X. Du, Q. Xue, H. Ding, Z. Li, Mechanochemical effects of ZnO powder in a wet super-fine grinding system as indicated by instrumental characterization, *Int. J. Miner. Process.*, 141 (2015) 15–19.
- [26] Y. Kadri, E. Srasra, I. Bekri-Abbess, P. Herrasti, Facile and eco-friendly synthesis of polyaniline/ZnO composites for corrosion protection of AA-2024 aluminium alloy, *J. Electroanal. Chem.*, 893 (2021) 115335, doi: 10.1016/j.jelechem.2021.115335.
- [27] S.P. Armes, J.F. Miller, Optimum reaction conditions for the polymerization of aniline in aqueous solution by ammonium persulphate, *Synth. Met.*, 22 (1988) 385–393.
- [28] S.A. Khayyat, M.S. Akhtar, A. Umar, ZnO nanocapsules for photocatalytic degradation of thionine, *Mater. Lett.*, 81 (2012) 239–241.
- [29] A. Becheri, M. Durr, P.L. Nostro, P. Baglioni, synthesis and characterization of zinc oxide nanoparticles: application of textiles as UV-absorbers, *J. Nanopart. Res.*, 10 (2008) 679–689.
- [30] H. Abdullah, N.P. Ariyanto, S. Shaari, B. Yulianto, S. Junaidi, Influence of structural and chemical properties on electron transport in mesoporous ZnO-based dye-sensitized solar cell, *Am. J. Eng. Appl. Sci.*, 2 (2009) 236–240.
- [31] K. Kakiuchi, E. Hosono, T. Kimura, H. Imai, S. Fujihara, Fabrication of mesoporous ZnO nanosheets from precursor templates grown in aqueous solutions, *J. Sol-Gel Sci. Technol.*, 39 (2006) 63–72.
- [32] V. Eskizeybek, F. Sari, H. Gulce, A. Gulce, A. Avci, Preparation of the new polyaniline/ZnO nanocomposite and its photocatalytic activity for degradation of methylene blue and malachite green dyes under UV and natural sun lights irradiations, *Appl. Catal., B*, 119–120 (2012) 197–206.
- [33] M. Alam, N.M. Alandis, A.A. Ansari, M.R. Shaik, Optical and electrical conducting properties of polyaniline/tin oxide nanocomposite, *J. Nanomater.*, 6 (2013) 1–5.
- [34] A. Mostafaei, A. Zolriasatein, Synthesis and characterization of conducting polyaniline nanocomposites containing ZnO nanorods, *Prog. Nat. Sci.: Mater. Int.*, 22 (2012) 273–280.
- [35] K.G.B. Alves, J.F. Felix, E.F. de Melo, C.G. dos Santos, C.A.S. Andrade, C.P. de Melo, Characterization of ZnO/polyaniline nanocomposites prepared by using surfactant solutions as polymerization media, *J. Appl. Polym. Sci.*, 125 (2011) 141–147.
- [36] S. Rajamanickam, S.M. Mohammad, Z. Hassan, Effect of zinc acetate dihydrate concentration on morphology of ZnO seed layer and ZnO nanorods grown by hydrothermal method, *Colloid Interface Sci. Commun.*, 38 (2020) 100312, doi: 10.1016/j.colcom.2020.100312.
- [37] R. Nosrati, A. Olad, R. Maramifar, Degradation of ampicillin antibiotic in aqueous solution by ZnO/polyaniline nanocomposite as photocatalyst under sunlight irradiation, *Environ. Sci. Pollut. Res.*, 19 (2012) 2291–2299.
- [38] D. Liu, Y. Lv, M. Zhang, Y. Liu, Y. Zhu, R. Zong, Y. Zhu, Defect-related photoluminescence and photocatalytic properties of porous ZnO nanosheets, *J. Mater. Chem. A*, 2 (2014) 15377–15388.
- [39] Z. Pei, L. Ding, M. Lu, Z. Fan, S. Weng, J. Hu, P. Liu, Synergistic effect in polyaniline-hybrid defective ZnO with enhanced photocatalytic activity and stability, *J. Phys. Chem. C*, 118 (2014) 9570–9577.
- [40] X. Xia, Q. Hao, W. Lei, W. Wang, D. Sun, X. Wang, Nanostructured ternary composites of graphene/Fe₃O₄/polyaniline for high-performance supercapacitors, *J. Mater. Chem.*, 22 (2012) 16844–16850.
- [41] N. Salah, S.S. Habib, Z.H. Khan, A. Memic, A. Azam, E. Alarfaj, N. Zahed, S. Al-Hamedi, High-energy ball milling technique for ZnO nanoparticles as antibacterial material, *Int. J. Nanomed.*, 6 (2011) 863–869.
- [42] L. Yu, W. Guo, M. Sun, J. He, Effect of grinding on the photocatalytic activity of commercial ZnO powder, *Adv. Mater. Res.*, 785–786 (2013) 498–501.
- [43] I. Sedenkova, M. Trchova, J. Stejskal, Thermal degradation of polyaniline films prepared in solutions of strong and weak acids and in water-FTIR and Raman spectroscopic studies, *Polym. Degrad. Stab.*, 93 (2008) 2147–2157.
- [44] S. Abbasi, M.S. Ekrami-Kakhki, The influence of ZnO nanoparticles amount on the optimisation of photo degradation of methyl orange using decorated MWCNTs, *Prog. Ind. Ecol.*, 13 (2019) 3–15.
- [45] S. Abbasi, Adsorption of dye organic pollutant using magnetic ZnO embedded on the surface of graphene oxide, *J. Inorg. Organomet. Polym. Mater.*, 30 (2020) 1924–1934.
- [46] M. Wondwossen, Y. Op, K. Tesfahun, Photocatalytic removal of methyl orange dye by polyaniline modified ZnO using visible radiation, *Sci. Technol. Arts Res. J.*, 2 (2014) 93–102.
- [47] S.M. El-Khouly, G.M. Mohamed, N.A. Fathy, G.A. Fagal, Effect of nanosized CeO₂ or ZnO loading on adsorption and catalytic properties of activated carbon, *Adsorpt. Sci. Technol.*, 35 (2017) 1–15, doi: 10.1177/0263617417698704.
- [48] H.K. Farag, R.M.M. Aboelenin, N.A. Fathy, Photodegradation of methyl orange dye by ZnO loaded onto carbon xerogels composites, *Asia-Pac. J. Chem. Eng.*, 12 (2017) 4–12.
- [49] J. Han, H.Y. Zeng, S. Xu, C.R. Chen, X.J. Liu, Catalytic properties of CuMgAlO catalyst and degradation mechanism in CWPO of methyl orange, *Appl. Catal. A*, 527 (2016) 72–80.